

Spatial Proportional Hazards Model with Differential Regularization

Lorenzo Tedesco

October 31, 2024

Abstract

This paper presents a semiparametric proportional hazards model designed to handle spatially varying covariate functions, applicable to both geostatistical and areal data observed on irregular spatial domains. The model is estimated through the maximization of a penalized partial likelihood, with a roughness penalty term based on a differential of the spatial field over the target domain. The finite element method is employed for efficient estimation, enabling a piecewise polynomial surface representation of the spatial field. We apply this method to analyze response time data from the London Fire Brigade.

Keywords: spatial proportional hazards model, differential regularization, semiparametric model, geostatistical data, areal data, finite element method, spatial field, survival analysis

1 Introduction

Survival analysis has long been an essential tool across various fields, including medicine, engineering, and social sciences, for analyzing time-to-event data. In this paper, we focus on one of the most widely used models within survival analysis: the Proportional Hazards (PH) model, first introduced by [Cox \(1972\)](#). The PH model assesses how covariates influence the hazard, or risk, of an event happening at any given moment in time, relative to a baseline risk. This model operates under the assumption that the effect of each covariate is proportional and constant over time, meaning that covariates alter the hazard rate by a multiplicative factor, without assuming a specific underlying time distribution for the event.

In recent years, survival analysis has advanced significantly in modeling various dependencies within survival data. Much research has focused on the relationship between censoring and time variables [Dereska and Keilegom \(2024\)](#), a critical aspect when handling censored data. However, other forms of dependence have received comparatively less attention. This paper addresses a scenario where the occurrence of an event is linked to its geographic location, thereby introducing spatial dependence into the analysis. Specifically, the probability of an event may be influenced by spatial characteristics associated with the event's location. We call the Proportional Hazards model that incorporates these spatial factors as the Spatial Proportional Hazards (SPH) model.

Spatial factors can generally be categorized into two main approaches: the geostatistical approach, which uses geographic coordinates (latitude and longitude), and the lattice approach, which considers the relative position of an area to neighboring regions, and our method is able to deal with both the framework.

A comprehensive literature review, including Bayesian approaches, is available in [Hanson and Zhou \(2014\)](#). In this work, however, we focus on a frequentist approach to the SPH model, for which various inference methods have been developed. Examples include the semiparametric estimating equations method by [Li and Lin \(2006\)](#) and the composite likelihood method by [Paik and Ying \(2012\)](#). A significant limitation of these methods is their reliance on a dependence structure that accounts only for the distance between locations, ignoring the domain's shape. This approach can lead to inaccuracies, especially when spatial dependence is influenced by the domain boundary.

Additionally, most semiparametric SPH models in the literature use a spline estimator to parameterize the baseline hazard function as infinite-dimensional parameters, rather than leaving this component fully unspecified, as in Cox's traditional partial likelihood approach ([Cox, 1972](#)). This additional parameterization requires estimating more parameters, leading to reduced robustness and accuracy in the estimation process.

In contrast, our method is grounded in the traditional partial likelihood approach, focusing specifically on the key multiplicative component of the model. Unlike other methodologies that introduce spatial dependence through a frailty-based approach—where the spatial domain is clustered and each cluster has a distinct effect on the hazard following a specified distribution—we incorporate a non-parametric spatial field defined over the entire domain to capture spatial dependence in the data.

For the estimation, we propose a novel method that leverages recent advancements in differential regularization, as discussed by [Wilhelm and Sangalli \(2016\)](#). A key advantage of our approach is its capacity to accommodate domains with complex shapes, such as those characterized by strong concavities or holes, where the domain geometry significantly impacts the behavior of the observed phenomenon.

We demonstrate that the methodology introduced in [Wilhelm and Sangalli \(2016\)](#), which concerns a generalized regression model for spatially distributed data when the response variable has a distribution within the exponential family, can be extended to a spatial proportional hazard model with randomly right-censored data. Specifically, we optimize a penalized log-likelihood function that includes a roughness penalty term based on a differential quantity of the spatial field, calculated over the domain of interest. This approach utilizes the so called Generalized Spatial Regression with PDE penalization (GSR-PDE) method ([Wilhelm and Sangalli, 2016](#)). Our proposed models leverage finite element methods on a triangulation of the domain to achieve precise estimates of the spatial field.

The paper is organized as follows: In [Section 2](#), we introduce the Spatial Proportional Hazards model. [Section 3](#) discusses the functional version of the PIRLS, tailored to our specific case of interest. In [Section 4](#), we describe the numerical implementation of the method using the finite element method. [Section 5](#) specifies the model version adapted for areal data. [Section 6](#) is dedicated to simulation studies, and [Section 7](#) presents an empirical application of the method. Finally, [Section 8](#) provides the conclusions. All technical details and proofs are deferred to the Appendix.

2 Model

We consider a bounded domain $\Omega \subset \mathbb{R}^2$ with a boundary $\partial\Omega$ that is regular and belongs to $C^2(\mathbb{R}^2)$. Let $\mathbf{p}_1, \dots, \mathbf{p}_n \in \Omega$ denote n points, where $\mathbf{p}_i = (p_{1i}, p_{2i})$. Each point \mathbf{p}_i is associated with a time-to-event random variable T_i . Due to censoring, T_i cannot be observed directly; instead, we obtain a realization of (Y_i, Δ_i) , denoted by (y_i, δ_i) , where $Y_i = \min(T_i, C_i)$, $\Delta_i = I(T_i \leq C_i)$, C_i is a censoring random variable, and $I(\cdot)$ is the indicator function. Additionally, we observe a covariate vector $\mathbf{x}_i \in \mathbb{R}^q$ at each location p_i . We assume that T_i is independent of C_i conditional on \mathbf{x}_i . We use a proportional hazard model for the random variables $\{T_i\}_{i=1}^n$. Specifically, let $\lambda_i(t | \mathbf{x})$ denote the conditional hazard function of T_i given $\mathbf{x}_i = \mathbf{x}$. We assume that

$$\lambda_i(t | \mathbf{x}) = \lambda_0(t) \exp(\mathbf{x}^\top \boldsymbol{\beta} + f(\mathbf{p}_i)), \quad (1)$$

where λ_0 is the unspecified baseline hazard, $\boldsymbol{\beta} \in \mathbb{R}^q$ is a vector of regression coefficients, and f is a smooth function from Ω to \mathbb{R} belonging to a suitable functional space \mathcal{F} . Thus, we will interpret the model in terms of hazards: the vector of coefficients $\boldsymbol{\beta}$ quantifies the influence of the covariates \mathbf{x}_i on the hazard function, so each component of $\boldsymbol{\beta}$ can be interpreted as the log hazard ratio associated with a one-unit increase in the corresponding covariate, holding other factors constant. The function $f(\mathbf{p}_i)$, instead, captures the spatial variation in hazards that is not accounted for by the covariates. Specifically, $f(\mathbf{p}_i)$ allows for the identification of localized risk factors affecting the hazard at different points in the domain, revealing areas with higher or lower risks relative to the baseline hazard $\lambda_0(t)$. Thus, the interpretation of hazards is twofold: it incorporates covariate effects via $\boldsymbol{\beta}$ and captures residual spatial variation through $f(\mathbf{p})$, providing a comprehensive view of risk that addresses both individual and spatial heterogeneity.

Note that f is identifiable up to an additive constant, so we assume that \mathcal{F} contains only functions such that at a given point $\mathbf{p}^* \in \Omega$ it holds $f(\mathbf{p}^*) = 0$. Note that alternative identifiability conditions can be considered, such as $\int_{\Omega} f = 1$. We propose to estimate the regression coefficients $\boldsymbol{\beta} \in \mathbb{R}^q$ and the spatial field $f \in \mathcal{F}$ by maximizing a penalized log-partial-likelihood functional:

$$\mathcal{L}_p(\boldsymbol{\beta}, f) = \mathcal{L}(\boldsymbol{\beta}, f) - \mu \int_{\Omega} (\Delta f(\mathbf{p}))^2 dp, \quad (2)$$

where $\mathcal{L}(\boldsymbol{\beta}, f)$ is the standard log-partial-likelihood for the PH model, defined as

$$\mathcal{L}(\boldsymbol{\beta}, f) = \sum_{i:\delta_i=1} \left(\mathbf{x}_i^\top \boldsymbol{\beta} + f(p_i) - \log \sum_{j:y_j \geq y_i} \exp(\mathbf{x}_j^\top \boldsymbol{\beta} + f(p_j)) \right). \quad (3)$$

Here, μ is a positive smoothing parameter, and the Laplacian $\Delta f = \frac{\partial^2 f}{\partial p_1^2} + \frac{\partial^2 f}{\partial p_2^2}$ measures the local curvature of the field f . A higher μ controls the wiggleness of f , while a smaller μ allows for more flexibility in f .

We show that maximizing the penalized log-likelihood function (2) is equivalent to minimizing the penalized least-squares functional considered in Sangalli et al. (2013). The quadratic form of this functional allows for an analytical characterization of its minimum (or equivalently, the maximum of the penalized log-likelihood functional), and thus for the estimation of $\hat{\boldsymbol{\beta}} \in \mathbb{R}^q$ and $\hat{f} \in \mathcal{F}$. As in Wilhelm and Sangalli (2016), which considers an exponential family, we cannot directly apply the standard PIRLS algorithm developed by O’Sullivan et al. (1986) for maximizing a penalized log-likelihood functional in generalized additive models. This is because the penalized log-likelihood in (2) involves a function parameter, the spatial field f , and the maximization occurs over the space $\mathbb{R}^q \times \mathcal{F}$, where \mathcal{F} is infinite-dimensional. Instead we recall the functional version of the PIRLS algorithm proposed in Wilhelm and Sangalli (2016) to find an approximate solution to the estimation problem.

3 Functional version of the PIRLS algorithm

We consider the more general penalized log-likelihood function given by:

$$\mathcal{L}_p(\boldsymbol{\beta}, f) = \mathcal{L}(\boldsymbol{\beta}, f) - \frac{\mu}{2} m(f, f), \quad (4)$$

where \mathcal{L} denotes the log-likelihood and $m(\cdot, \cdot) : \mathcal{F} \times \mathcal{F} \rightarrow \mathbb{R}$ is a bilinear, symmetric, and semi-positive definite form. This formulation enables us to extend the PIRLS algorithm to accommodate any functional roughness penalty of this general quadratic form.

For that, define the following quantities:

$$\begin{aligned} \theta_i(\boldsymbol{\beta}, f) &= \exp(\mathbf{x}_i^\top \boldsymbol{\beta} + f(p_i)), \\ r_{ji} &= I(Y_j \geq Y_i), \\ s_i(\boldsymbol{\beta}, f) &= \sum_{j=1}^n r_{ji} \theta_j(\boldsymbol{\beta}, f), \\ l_i(\boldsymbol{\beta}, f) &= \sum_{j=1}^n r_{ij} \frac{\delta_j}{s_j(\boldsymbol{\beta}, f)}, \\ v_i(\boldsymbol{\beta}, f) &= \theta_i(\boldsymbol{\beta}, f) / l_i(\boldsymbol{\beta}, f). \end{aligned}$$

First, we show that the problem of maximizing (4) is equivalent to minimizing the following functional $\mathcal{J}_\mu(\boldsymbol{\beta}, f)$ with respect to $(\boldsymbol{\beta}, f)$:

$$\mathcal{J}_\mu(\boldsymbol{\beta}, f) = \|V^{-1/2}(\boldsymbol{\delta}/\mathbf{l} - \boldsymbol{\theta})\|^2 + \mu m(f, f),$$

where $\boldsymbol{\delta} = (\delta_1, \dots, \delta_n)^\top$, $\mathbf{l} = (l_1, \dots, l_n)^\top$, $\boldsymbol{\delta}/\mathbf{l} = (\delta_1/l_1, \dots, \delta_n/l_n)^\top$, and $V = \text{diag}(v_1, \dots, v_n)$, where such quantities are supposed to be constant. As, in fact, \mathbf{l} and V also depend on $(\boldsymbol{\beta}, f)$, this suggests an iterative scheme for the solution of the estimation problem. Let $(\boldsymbol{\beta}^{(k)}, f_n^{(k)})$ be the value of $(\boldsymbol{\beta}, f)$ after k iterations of the algorithm, and let $\boldsymbol{\theta}^{(k)}$ the estimate of the vector $\boldsymbol{\theta} = (\theta_1, \dots, \theta_n)^\top$ after k iterations, and define $\Theta^{(k)} = \text{diag}(\boldsymbol{\theta}^{(k)})$. Let X be the $q \times n$ matrix where the column i is equal to \mathbf{x}_i and define also $\mathbf{z}^{(k)} = (\Theta^{(k)})^{-1}(\boldsymbol{\delta}/\mathbf{l} - \boldsymbol{\theta}^{(k)}) + X^\top \boldsymbol{\beta}^{(k)} + f^{(k)}$, and let $W^{(k)}$ be the $n \times n$ diagonal matrix with i th entry equal to $v_i^{-1}(\boldsymbol{\beta}^{(k)}, f^{(k)}) \theta_i^2(\boldsymbol{\beta}^{(k)}, f^{(k)})$. The first order approximation of $\boldsymbol{\theta}(\boldsymbol{\beta}, f)$ in the neighborhood of the current

value of $\boldsymbol{\theta}^{(k)}$ has to be considered in the space $\mathbb{R}^q \times \mathcal{F}$ and yields to the following quadratic approximation of $\mathcal{J}_\mu(\boldsymbol{\beta}, f)$:

$$\tilde{\mathcal{J}}_\lambda^{(k)}(\boldsymbol{\beta}, f) = \left\| (W^{(k)})^{1/2}(\boldsymbol{z}^{(k)} - X^\top \boldsymbol{\beta} - f) \right\|^2 + \mu m(f, f). \quad (5)$$

We can consider the following iterative scheme:

1. Compute $\boldsymbol{z}^{(k)}$ and $W^{(k)}$ based on $(\boldsymbol{\beta}^{(k)}, f_n^{(k)})$.
2. Next, find $\boldsymbol{\beta}$ and f_n that minimize (5).
3. Perform the standard proportional hazards model estimation using X and $f_n^{(k)}$ as covariate and denote by $\hat{\boldsymbol{\beta}}$ and \hat{c} the resulting regression coefficient for X and $f_n^{(k)}$, respectively.
4. Define $\boldsymbol{\beta}^{(k+1)} = \hat{\boldsymbol{\beta}}$ and $f_n^{(k+1)} = \hat{c}(f_n^{(k)} - f_n^{(k)}(p^*))$.

Here $f_n^{(k)}(p^*)$ is the estimation of f at step k at p^* . The standardization of $f_n^{(k)}$ in step 4 ensures that $f_n(p^*) = 0$ and that (1) is satisfied. We can use a stopping criteria based on a sufficiently small variation of two successive values of (5) or a maximum number of iterations.

4 Numerical Implementation using the Finite Element Method

We now turn our attention to the scenario where the roughness penalty takes the form $m(f, f) = \int_\Omega (\Delta f(p))^2 dp$. In each iteration of the functional PIRLS algorithm, we aim to determine the values of $\boldsymbol{\beta} \in \mathbb{R}^q$ and $f \in \mathcal{F}$ that together minimize the expression:

$$\tilde{\mathcal{J}}_\lambda(\boldsymbol{\beta}, f) = \|W^{1/2}(z - X^\top \boldsymbol{\beta} - f_n)\|^2 + \lambda \int_\Omega (\Delta f)^2. \quad (6)$$

For simplicity, we omit the dependence on the iteration counter k in this notation and throughout the following sections. Let us now consider what type of space \mathcal{F} is suitable for the current problem. To do so, we introduce the Sobolev space $H^m(\Omega)$, which is a Hilbert space comprising all functions in $L^2(\Omega)$ along with all their distributional derivatives up to order m . Since the roughness penalty term $\int_\Omega (\Delta f)^2$ must be well-defined, it follows that $\mathcal{F} \subset H^2(\Omega)$. According to the Sobolev embedding theorem, $H^2(\Omega) \subset C^0(\Omega)$. Therefore, any function $f \in H^2(\Omega)$ is continuous and can be evaluated pointwise, allowing us to compute the vector f_n in the partial likelihood term. To ensure the uniqueness of the minimizer in (6), appropriate boundary conditions must be imposed. These conditions specify the desired behavior of the estimated function f at the boundaries of the domain of interest. Typically, constraints can be set on the value of f at the boundary $\partial\Omega$, i.e., $f|_{\partial\Omega} = \gamma_D$ (Dirichlet boundary conditions), or on the flux of the function through the boundary, i.e., $\partial_n f|_{\partial\Omega} = (\nabla f)^\top \mathbf{n} = \gamma_N$ (Neumann boundary conditions), where \mathbf{n} is the outward-pointing normal unit vector to the boundary, and $\nabla f = (\partial f/\partial p_1, \partial f/\partial p_2)^\top$ represents the gradient of f . If γ_D or γ_N are zero functions, the boundary conditions are said to be homogeneous. It is also possible to apply different boundary conditions to various parts of the boundary, forming a partition of $\partial\Omega$. To ensure the uniqueness of the minimization problem (4.1), we consider the space:

$$\mathcal{F} = H_n^2 = \{f \in H^2 \mid (\nabla f)^\top \mathbf{n} = 0 \text{ on } \partial\Omega\}.$$

For more details on general boundary conditions, see [Azzimonti et al. \(2014\)](#).

4.1 Characterization of the Solution to the Penalized Partial Likelihood Problem

We assume that the design matrix XX^\top is of full rank and that the weight matrix W contains strictly positive entries. Define $H = X(X^\top WX)^{-1}X^\top W$ and $Q = I - H$, where I is an identity matrix of the appropriate size. For any function u within the functional space $\mathcal{F} = H_n^2(\Omega)$, let $\mathbf{u}_n = (u(\mathbf{p}_1), \dots, u(\mathbf{p}_n))^\top$

denote the vector of evaluations of u at the n spatial locations $\{\mathbf{p}_i\}_{i=1}^n$. Let $\tilde{\boldsymbol{\beta}}$ and \tilde{f} denote the minimizers of the functional $\tilde{J}_\lambda(\boldsymbol{\beta}, f)$ in (6), and $\hat{\boldsymbol{\beta}}$ and \hat{f} the maximizers of the penalized partial likelihood functional $\mathcal{L}_p(\boldsymbol{\beta}, f)$ in (4). Under these conditions, the following proposition describes the minimizers $\tilde{\boldsymbol{\beta}}$ and \tilde{f} of the functional (6).

Proposition 1. *There exists a unique pair $(\tilde{\boldsymbol{\beta}}, \tilde{f}) \in \mathbb{R}^q \times H_n^2$ that minimizes (4). Furthermore,*

- $\tilde{\boldsymbol{\beta}} = (X^\top W X)^{-1} X^\top W(z - \tilde{f}_n)$, where $\tilde{\mathbf{f}}_n = (\tilde{f}(\mathbf{p}_1), \dots, \tilde{f}(\mathbf{p}_n))^\top$,
- \tilde{f} satisfies:

$$\mathbf{u}_n^\top Q \tilde{f}_n + \lambda \int_{\Omega} (\Delta u)(\Delta \tilde{f}) = \mathbf{u}_n^\top Q z, \quad \forall u \in H_n^2. \quad (7)$$

Using Proposition 1 and the functional version of the PIRLS algorithm from Section 3, we obtain a characterization of the maximum penalized log-likelihood within the functional space $H_n^2(\Omega)$.

4.2 Solution to the Penalized Partial Likelihood

Here, we outline the methodology for minimizing $\tilde{J}_\lambda(\boldsymbol{\beta}, f)$ with respect to both $\boldsymbol{\beta}$ and f . As indicated by Proposition 1, computing $\tilde{\boldsymbol{\beta}}$ is straightforward. The key challenge is to find \tilde{f} that satisfies (7). To address this, we introduce the space:

$$H_n^1 = \{f \in H^1 \mid (\nabla f)^\top \mathbf{n} = 0 \text{ on } \partial\Omega\}.$$

According to Wilhelm and Sangalli (2016); Sangalli et al. (2013), problem (7) is equivalent to finding $(\tilde{f}, \tilde{h}) \in H_n^1(\Omega) \times H_n^1(\Omega)$ such that

$$\begin{cases} \mathbf{u}_n^\top Q \tilde{f}_n - \lambda \int_{\Omega} (\nabla u)^\top \nabla \tilde{h} = \mathbf{u}_n^\top Q z, \\ - \int_{\Omega} (\nabla \tilde{f})^\top \nabla v = \int_{\Omega} \tilde{h} v, \end{cases} \quad (8)$$

for each $(u, v) \in H_n^1 \times H_n^1(\Omega)$. This formulation requires less regularity on the functions involved compared to formulation (6) defined in $H_n^2(\Omega)$. In the following section, we discuss how the finite element method can be employed to construct a finite-dimensional subspace of $H_n^1(\Omega)$, enabling the computation of an approximate solution to (7) within this space.

4.3 Finite Elements

The finite element method is a prevalent numerical technique in engineering for solving problems involving partial differential equations (Quarteroni and Quarteroni, 2009). To build a finite element space, we begin by dividing the domain of interest Ω into smaller subdomains. Common domain partitions include triangular meshes. We consider a regular triangulation \mathcal{T} of Ω , where adjacent triangles share either a vertex or an edge. The domain Ω is thus approximated by $\Omega_{\mathcal{T}}$, which is the union of all triangles. Consequently, the boundary $\partial\Omega$ is approximated by a polygon (or multiple polygons for domains with interior holes). This triangulation effectively captures the complex geometry of the domain, including significant concavities such as rivers and detailed structures like bridges that connect different parts of the city.

From this triangulation, locally supported polynomial functions are defined over the triangles, forming a set of basis functions ψ_1, \dots, ψ_K that span a finite-dimensional subspace \mathcal{F}_K of H_n^1 . Linear finite elements are created using a basis system where each basis function ψ_i is associated with a vertex ξ_i (for $i = 1, \dots, K$) of the triangulation \mathcal{T} . In particular, each basis function ψ_i is a piecewise linear polynomial that equals one at the vertex ξ_i and zero at all other vertices of the mesh, i.e., $\psi_i(\xi_j) = \delta_{ij}$ for all $i, j = 1, \dots, K$, where δ_{ij} is the Kronecker delta. Figure 1 provides an example of a linear finite element basis function on a planar mesh, highlighting its localized support.

Let $\boldsymbol{\psi} = (\psi_1, \dots, \psi_K)^\top$ be the column vector containing the K piecewise linear basis functions corresponding to the K vertices ξ_1, \dots, ξ_K . Any function h in the finite element space \mathcal{F}_K can be expressed as a linear combination of the basis functions ψ_1, \dots, ψ_K . Let $\mathbf{h} = (h_1, \dots, h_K)$ represent the coefficients of this basis expansion for \mathbf{h} , such that

$$h(\cdot) = \sum_{j=1}^K h_j \psi_j(\cdot) = \mathbf{h}^\top \boldsymbol{\psi}(\cdot).$$

Note that

$$h(\xi_i) = \sum_{j=1}^K h_j \psi_j(\xi_i) = \sum_{j=1}^K h_j \delta_{ij} = h_i,$$

therefore,

$$\mathbf{h} = (h(\xi_1), \dots, h(\xi_K)),$$

which shows that each function $h \in \mathcal{F}_K$ is completely determined by its values at the mesh nodes.

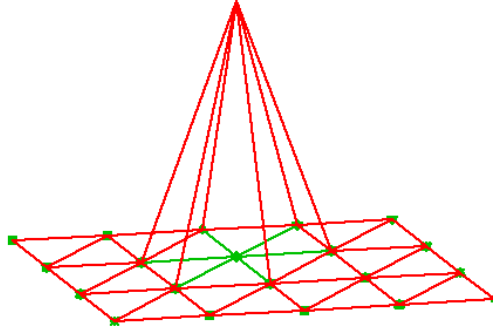


Figure 1: Example of a linear finite element basis function on a planar mesh. The function is locally supported, taking the value one at a specific vertex and zero at all other vertices of the mesh.

4.4 Numerical solution to the Penalized Partial Likelihood

The functions and integrals in equation (8) can be approximated using elements from the finite element space \mathcal{F}_K . As a result, the problem (8) is approximated by its discrete version: find $(\tilde{f}, \tilde{h}) \in \mathcal{F}_K \times \mathcal{F}_K$ such that (8) holds for all $(u, v) \in \mathcal{F}_K \times \mathcal{F}_K$, where the integrals are now computed over the triangulation $\Omega_{\mathcal{T}}$. Define Ψ as the $n \times K$ matrix representing the evaluations of the K basis functions at the n data locations $\mathbf{p}_1, \dots, \mathbf{p}_n$,

$$\Psi = \begin{bmatrix} \psi^\top(\mathbf{p}_1) \\ \vdots \\ \psi^\top(\mathbf{p}_n) \end{bmatrix} \quad (9)$$

and consider the $K \times K$ matrices

$$R_0 = \int_{\Omega_{\mathcal{T}}} (\psi \psi^\top), \quad R_1 = \int_{\Omega_{\mathcal{T}}} (\nabla \psi)^\top \nabla \psi.$$

Using this notation, for functions $\tilde{f}, \tilde{h}, u, v \in \mathcal{F}_K$, the integrals in (8) can be written as:

$$\int_{\Omega_{\mathcal{T}}} (\nabla u)^{\top} \nabla \tilde{h} = \mathbf{u}^{\top} R_1 \tilde{\mathbf{h}}, \quad \int_{\Omega_{\mathcal{T}}} (\nabla \tilde{f})^{\top} \nabla v = \tilde{\mathbf{f}}^{\top} R_1 \mathbf{v}, \quad \int_{\Omega_{\mathcal{T}}} \tilde{h} v = \tilde{\mathbf{h}}^{\top} R_0 \mathbf{v},$$

where $\tilde{\mathbf{f}}, \tilde{\mathbf{h}}, \mathbf{u}$, and \mathbf{v} are the coefficient vectors of the basis expansions of \tilde{f}, \tilde{h}, u , and v , respectively. Consequently, the discrete version of problem (8) reduces to solving a linear system, as formulated in the following proposition.

Proposition 2. *The discrete form of (8) is given by the system*

$$\begin{bmatrix} -\Psi^{\top} Q \Psi & \lambda R_1 \\ \lambda R_1 & \lambda R_0 \end{bmatrix} \begin{bmatrix} \tilde{\mathbf{f}} \\ \tilde{\mathbf{h}} \end{bmatrix} = \begin{bmatrix} -\Psi^{\top} Q \mathbf{z} \\ \mathbf{0} \end{bmatrix}, \quad (10)$$

which has a unique solution pair $(\tilde{\mathbf{f}}, \tilde{\mathbf{h}})$ corresponding to the coefficients of the basis expansions of \tilde{f} and \tilde{h} .

Proof. The uniqueness of the solution to (10) is guaranteed by the positive definiteness of the matrices R_0 and $(\Psi^{\top} Q \Psi + \lambda R_1 R_0^{-1} R_1)$. \square

Let $P = R_1 R_0^{-1} R_1$ and $S = \Psi(\Psi^{\top} Q \Psi + \lambda P)^{-1} \Psi^{\top} Q$. Using the functional form of the PIRLS algorithm, and leveraging Propositions 1 and 2, we obtain the following expressions for the maximizers $\hat{\beta}$ and \hat{f} of the penalized partial likelihood (2):

$$\hat{\beta} = (X^{\top} W X)^{-1} X^{\top} W (I - S) \mathbf{z},$$

with \hat{f} identified by the vector

$$\hat{\mathbf{f}} = (\Psi^{\top} Q \Psi + \lambda P)^{-1} \Psi^{\top} Q \mathbf{z},$$

and the vector of evaluations of \hat{f} at the n data locations given by

$$\hat{\mathbf{f}}_n = \Psi \hat{\mathbf{f}} = \Psi (\Psi^{\top} Q \Psi + \lambda P)^{-1} \Psi^{\top} Q \mathbf{z} = S \mathbf{z},$$

where the vector of pseudo-data \mathbf{z} , and the matrices W, Q , and S are those obtained upon convergence of the PIRLS algorithm.

The positive definite matrix P represents the discretization of the penalty term in (2) and (7). Due to the variational formulation (8) of the estimation problem, this penalty matrix does not require the computation of second-order derivatives. Azzimonti et al. (2014) demonstrates that in the finite element space used for discretization, P is equivalent to the penalty matrix that would result from a direct discretization of the penalty term in (2) and (7), which would otherwise involve the computation of second-order derivatives.

4.5 Selecting the Parameter μ Using Cross-Validation

When it comes to choosing the parameter μ , one straightforward approach is a visual inspection. This method allows the researcher to select a value that achieves the desired smoothness of the estimated spatial field. However, to avoid subjective decision-making, we propose a more objective, numerical method. Following the approach of Cygu et al. (2021), we can utilize cross-validation to determine the optimal value of μ . Specifically, we select the μ that results in the lowest cross-validated partial likelihood deviance (CV-PLD) or the highest cross-validated Harrell's concordance index (CV-C-index) (Harrell Jr et al., 1996).

To compute the CV-PLD for each μ , we employ k -fold cross-validation. This process involves splitting the training data into k subsets (folds), training the model on $k - 1$ folds, and validating it on the remaining fold. This procedure is repeated k times, each time with a different fold serving as the validation set. We use two metrics for this purpose: CV-PLD and CV-C-index (Dai and Breheny, 2019). The CV-PLD is defined as:

$$\text{CV-PLD}(\mu) = -2 \sum_{k=1}^K \left(\mathcal{L}(\hat{\beta}_{-k}(\mu), \hat{f}_{-k}(\mu)) - \mathcal{L}_{-k}(\hat{\beta}_{-k}(\mu), f_{-k}(\mu)) \right), \quad (11)$$

where $\mathcal{L}(\hat{\beta}_{-k}(\mu), \hat{f}_{-k}(\mu))$ represents the log partial likelihood evaluated at $(\hat{\beta}_{-k}, \hat{f}_{-k}(\mu))$ using the entire dataset, and $\mathcal{L}_{-k}(\hat{\beta}_{-k}(\mu), \hat{f}_{-k}(\mu))$ is the log partial likelihood evaluated at $(\hat{\beta}_{-k}, \hat{f}_{-k}(\mu))$ on the retained data (all but the excluded fold). The $(\hat{\beta}_{-k}, \hat{f}_{-k}(\mu))$ values denote the penalized estimates derived from the retained data. The optimal value of μ is the one that minimizes (11). Notably, equation (11) typically provides superior results compared to simply evaluating the partial likelihood on the held-out fold (a method sometimes referred to as the basic approach), as the likelihood of any given observation is influenced by the other elements in the risk set.

The alternative cross-validation metric, the CV-C-index, is based on Harrell’s concordance index for Cox models. This metric, known as the cross-validated C-index, calculates the probability that, for a random pair of individuals, the predicted survival times are correctly ordered according to their actual survival times. This method is similar to the implementation available in the `survival` package (Therneau et al., 2015).

5 Model Version for Areal data

6 Simulation Results

To demonstrate the performance of the proposed model, we present simulations on a horseshoe domain, as defined in Ramsay (2002); Wood et al. (2008). We use the spatial field $f(x, y)$, depicted in Figure 2a and defined as follows:

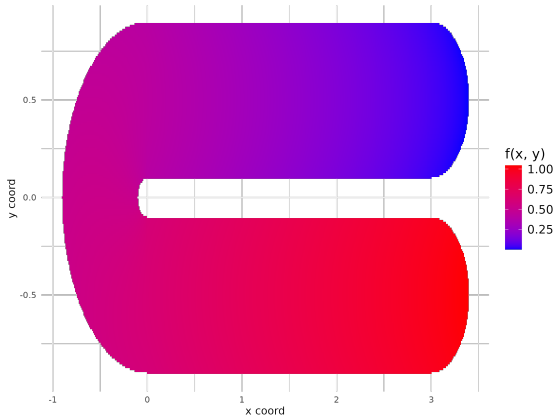
$$f(x, y) = \begin{cases} -\frac{1}{8} \left(x + \frac{\pi r}{2} + (y - r)^2 + 10 \right) + c & \text{if } (x - 3)^2 + (y - r)^2 \leq (r - r_0)^2 \text{ and } x \geq 3, \\ -\frac{1}{8} \left(x + \frac{\pi r}{2} + (y - r)^2 + 10 \right) + c & \text{if } 0 \leq x \leq 3, r_0 \leq y \leq 2r - r_0, \\ -\frac{1}{8} \left(\arctan\left(-\frac{y}{x}\right) r + \left(\sqrt{x^2 + y^2} - r\right)^2 + 10 \right) + c & \text{if } r_0^2 \leq x^2 + y^2 \leq (2r - r_0)^2 \text{ and } x < 0, \\ -\frac{1}{8} \left(-x - \frac{\pi r}{2} + (-y - r)^2 + 10 \right) + c & \text{if } 0 \leq x \leq 3, -(2r - r_0) \leq y \leq -r_0, \\ -\frac{1}{8} \left(-x - \frac{\pi r}{2} + (-y - r)^2 + 10 \right) + c & \text{if } (x - 3)^2 + (y + r)^2 \leq (r - r_0)^2 \text{ and } x > 3, \\ 0 & \text{otherwise,} \end{cases}$$

where $r = 0.5$ and $r_0 = 0.1$, and c is a constant chosen so that the minimum value of f over the horseshoe domain is zero, approximately $c \simeq 1.77$. Figure 2a shows the values of the spatial field over the horseshoe.

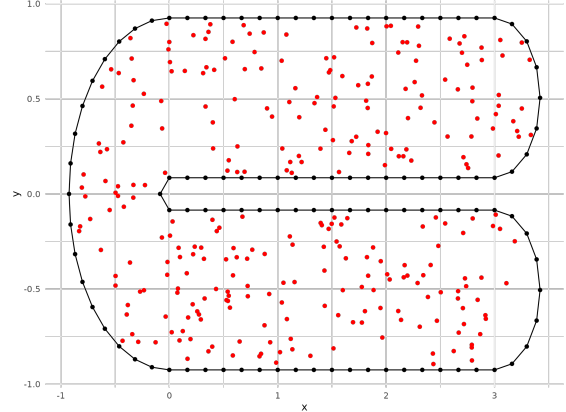
6.1 Geostatistical Data

We randomly sample $n = 100, 200, 300$ points, denoted by $\{p_i\}_{i=1}^n$, from the horseshoe domain, as illustrated in Figure 2b. Figure 2c shows the corresponding Delaunay triangulation (Shewchuk, 2002). Each sampled point is associated with an observation x_i of a unidimensional random variable X_i , for which we omit the bold notation, and that follows a standard normal distribution. Additionally, we observe (y_i, δ_i) , where $y_i = \min(T_i, C_i)$ and $\delta_i = I(T_i \leq C_i)$. The variable T_i given $X_i = x$ follows a proportional hazards model with baseline hazard $\lambda_0(t) = 1$ and $\beta_0 = 0.2$, as defined in equation (1), with the form $\lambda(t|x) = \lambda_0(t) \exp(x\beta_0 + f(p_i))$. This implies that the random variable T_i at location $\pm p_i$ follows an exponential distribution with rate (inverse of the mean) $\exp(x\beta_0 + f(p_i))$.

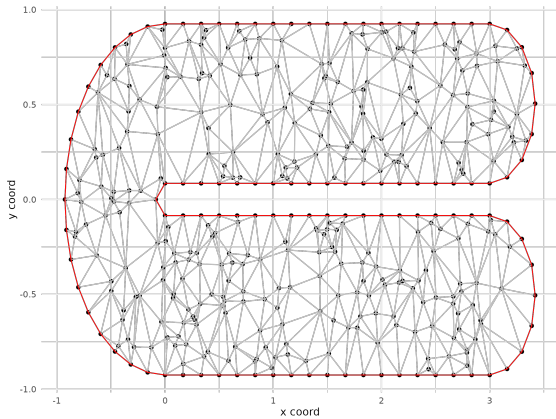
To introduce censoring, we set $C_i = 1$ for each i , resulting in approximately 20% censored observations. We set $\mu = 0.5, 1, 5, 10$ in order to understand how the value of μ affects the estimation of the spatial field f and of the regression coefficients vector of β . The finite elements method is applied using a basis of order 1 constructed on the Delaunay triangulation over the sampled locations. We conduct $N = 250$ simulations for each combination of n and μ . An example of the estimated spatial field is given in Figure 2d.



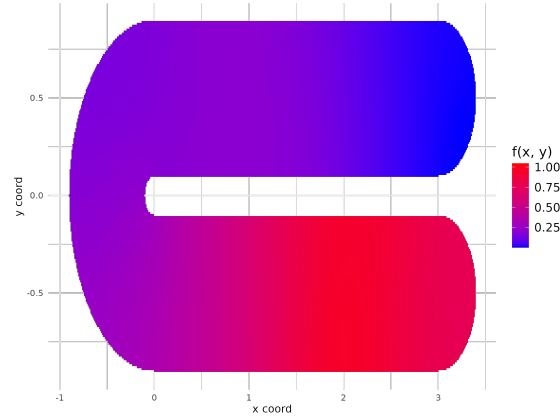
(a) Spatial field $f(\mathbf{p})$ over the horseshoe domain



(b) Example of sample points over the horseshoe domain for $n = 300$.



(c) Mesh based on the sampled points of Figure 2b.



(d) Example of estimation of the spatial field based on the sampled points of Figure 2b and setting $\mu = 10$.

Figure 2: Figures illustrating various aspects of the spatial field and sampling.

We report in Table 1 the simulation results that highlights how changes in the smoothing parameter μ , censoring levels, and sample sizes affect key performance metrics. The bias values for β remain close to zero across most scenarios, indicating unbiased estimates, with slight variations at higher levels of μ . The standard deviation (Sd) decreases as the sample size n increases, suggesting that larger samples improve estimate stability. Additionally, the 95% confidence interval coverage probability (CP95) stays close to the nominal level, particularly in larger samples, supporting the reliability of interval estimates.

For the spatial field f , we reported the Mean Squared Error (MSE) defined as $\text{MSE} = n^{-1} \sum_{i=1}^n (\hat{f}(\mathbf{p}_i) - f(\mathbf{p}_i))^2$, as a performance metric. We observe that the MSE values generally decrease as n grows, suggesting improved precision with more data. Higher censoring percentages (e.g., 40%) introduce a slight increase in MSE and its standard deviation (Sd MSE), indicating reduced accuracy under increased censoring.

μ	Cens. %	n	Regression coefficient β			Spatial field f	
			bias	Sd	CP95	MSE	Sd MSE
0.5	20%	100	-0.001	0.121	0.944	0.177	0.125
		200	-0.010	0.078	0.964	0.155	0.111
	40%	100	-0.002	0.145	0.944	0.227	0.222
		200	-0.013	0.091	0.960	0.150	0.096
1	20%	100	-0.001	0.122	0.944	0.172	0.126
		200	-0.010	0.077	0.968	0.157	0.121
	40%	100	-0.003	0.145	0.932	0.206	0.171
		200	-0.012	0.091	0.960	0.153	0.110
3	20%	100	-0.001	0.121	0.948	0.177	0.146
		200	-0.009	0.077	0.972	0.158	0.137
	40%	100	-0.003	0.145	0.936	0.206	0.178
		200	-0.012	0.091	0.964	0.155	0.128
5	20%	100	-0.001	0.121	0.948	0.185	0.164
		200	-0.009	0.077	0.972	0.161	0.146
	40%	100	-0.003	0.145	0.940	0.216	0.196
		200	-0.011	0.090	0.964	0.159	0.141
10	20%	100	-0.002	0.121	0.948	0.196	0.177
		200	-0.008	0.077	0.972	0.166	0.163
	40%	100	-0.002	0.145	0.940	0.229	0.217
		200	-0.010	0.090	0.964	0.163	0.157

Table 1: Simulation results for estimating the regression coefficient β and spatial field f across different values of the smoothing parameter μ , varying censoring percentages (Cens. %) and sample sizes n . The performance metrics include bias, standard deviation (Sd), and 95% confidence interval coverage probability (CP95) for β , as well as mean squared error (MSE) and standard deviation of MSE (Sd MSE) for f . The results demonstrate the impact of μ , censoring level, and sample size on the precision and accuracy of the estimates.

6.2 Areal Data

//TODO

7 Empirical Application

In this section, we apply the proposed method to analyze the London Fire Brigade (LFB) response time data. The dataset is available in the R package `spatsurv` (Taylor and Rowlingson, 2017) and is further explored in Taylor (2017). The original data can also be accessed via the London Datastore Fire and Authority (2015). Our analysis focuses on data from 2009, specifically on fires occurring in residential dwellings, as these are associated with the highest number of fatalities. The response variable of interest is the time taken for the first fire engine to arrive at the scene of a dwelling fire. We excluded observations where the response time was missing, and the resulting dataset contains no censored data.

In Figure 3, we display the observed locations of these incidents, highlighting the spatial distribution of fires across London. The blue dots represent the locations of the observed fires, while the grey boundary outlines the geographical area under study. As can be seen from the image, the area excludes the River Thames, which corresponds to a natural boundary that could potentially influence the arrival time of the first fire engine. Given the irregular path of the river, it was necessary to smooth the boundary of the domain. After smoothing the domain and excluding points that fall into the river or outside the region of interest, the dataset results in 6657 observed locations, though less than 0.01% of the points were omitted. Some observations had identical locations, and while different strategies could be used, such as jittering the points, we chose to randomly omit the duplicated locations. This led to a dataset of 5949 unique locations, resulting in the removal of approximately 10% of the data points, which still leaves a sufficiently large dataset

for analysis.

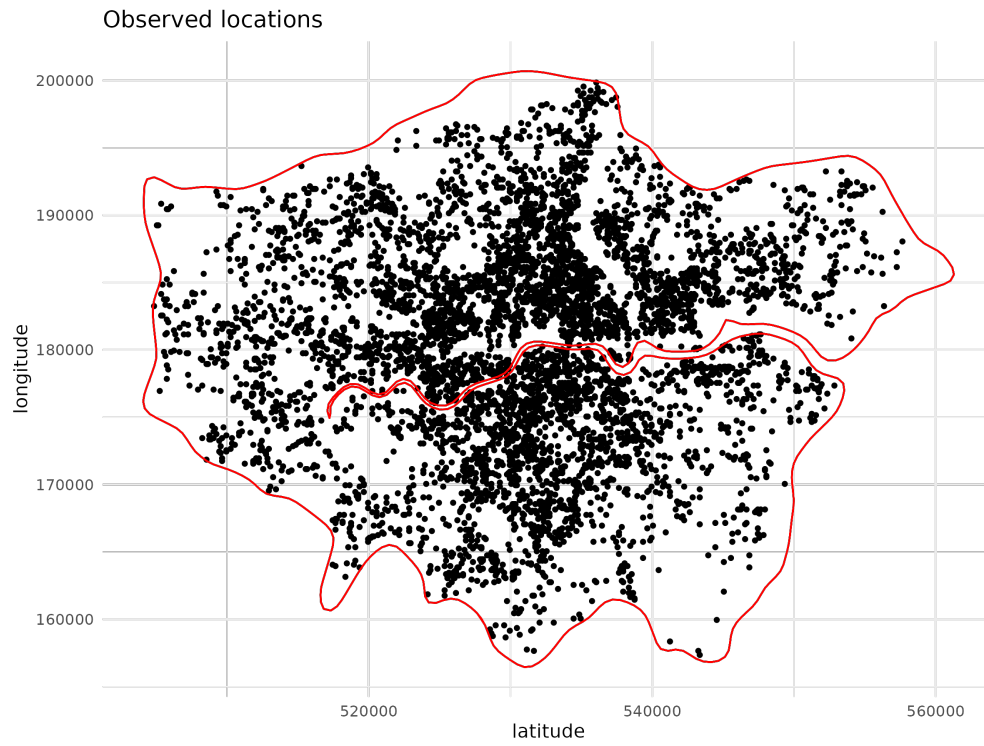


Figure 3: Observed fire locations in London. The blue points represent the geographical locations of fire incidents in residential dwellings across the city. The red border outlines the area under study, excluding the River Thames as a natural boundary.

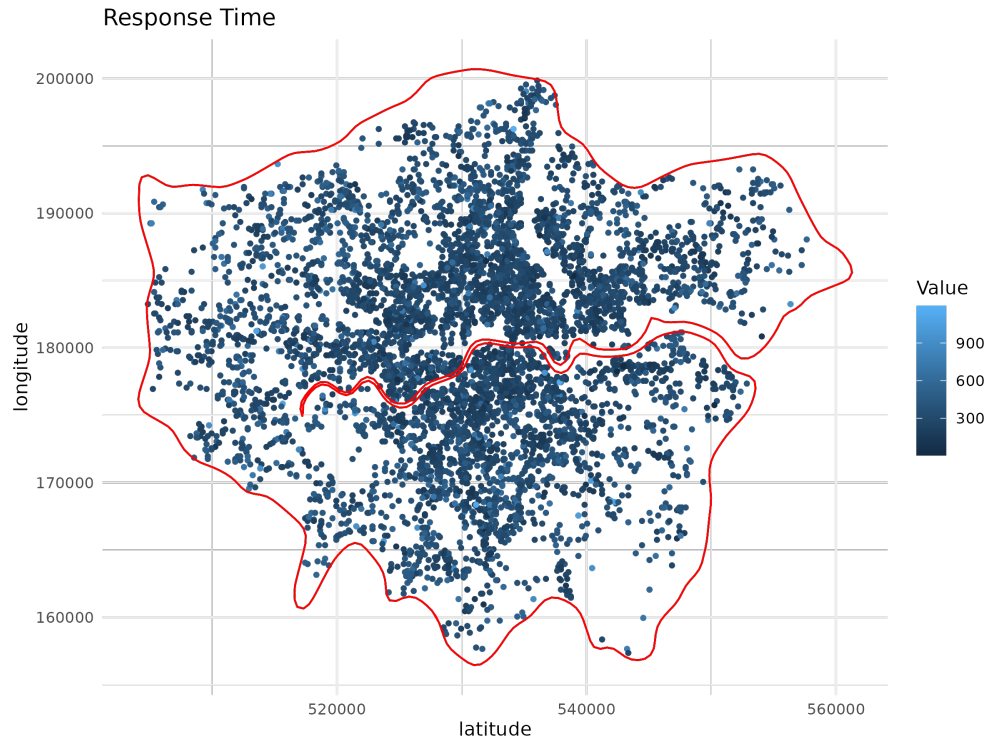


Figure 4: Distribution of observed response times of the first fire engine to reach fire incidents. The color intensity represents the density of the response times across different locations.

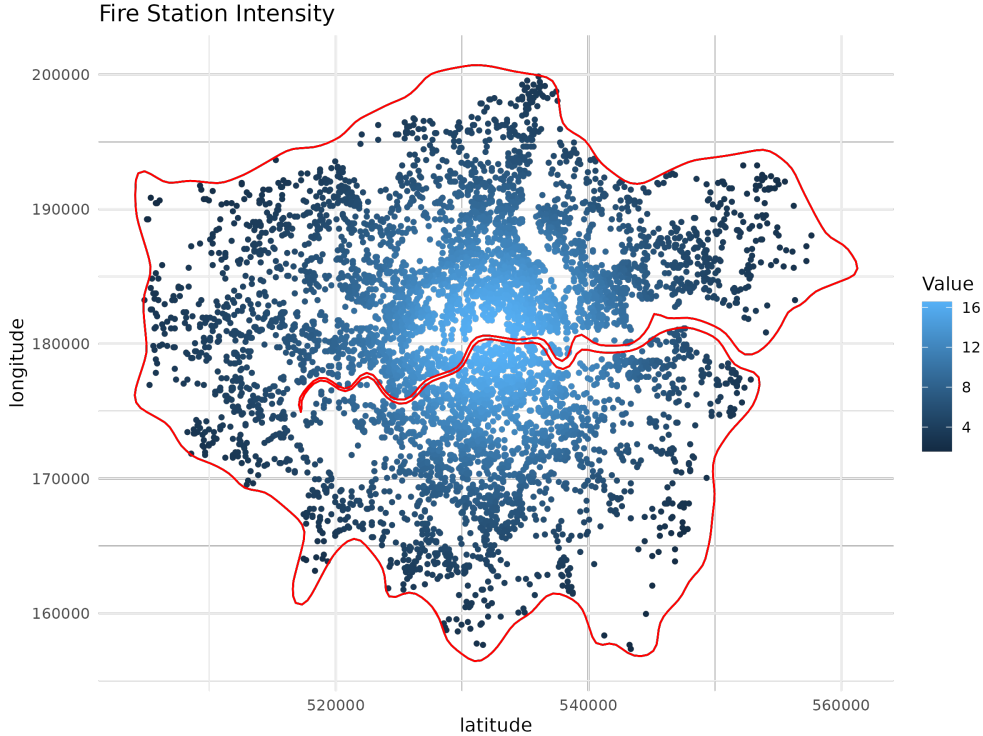


Figure 5: Fire station intensity map. The blue intensity highlights the estimated proximity of fire stations to the observed fire locations, with red contours indicating areas of higher station density.

It is reasonable to expect that the response time to a fire service call is influenced by the proximity of the nearest fire station. However, in practice, the closest station may already be responding to another incident. As explored in [Taylor and Rowlingson \(2017\)](#), we include a scaled fire station intensity measure as a covariate in the model, which accounts for the proximity of fire stations to fire locations. A mesh was constructed based on the observed locations using first-order basis functions. To determine the smooth parameter $\mu \in \{1, 4, 7, \dots, 100\}$, we applied the CV-PLD method discussed in [Section 4.5](#), utilizing a 10-fold cross-validation approach. The optimal μ was found to be 46. The estimation algorithm terminates if the Euclidean norm difference between consecutive estimates of the spatial field is less than 0.01, with convergence typically occurring within 5 iterations. The estimated regression coefficient for the fire station density covariate is $\beta = 0.0667$, with a standard deviation of 1.41×10^{-5} , indicating a statistically significant effect at the 1% level.

In [Figure 6](#), we present the estimated spatial field. The figure highlights how the river acts as a natural boundary, constraining the fire engines' ability to respond promptly to incidents on the opposite side of its banks. This observation suggests that geographical features significantly impact response efficiency and should be carefully considered when interpreting spatial variations in the data.

In [Figure 7](#), we provide a cross-section of the spatial field, highlighted as a vertical line in [Figure 6](#). This cross-section shows the estimated value of the spatial field at longitude 535000 as a function of latitude. We observe a distinct change point around latitude 180000, corresponding to the river's location, where the hazard level immediately drops by approximately 80%.

It is arguable that the river effect might be artificially induced by omitting the river space from the domain and that the presence of bridges along the boundary effectively mitigated issues related to water. While the choice of domain should ideally be guided by a priori knowledge about the specific problem, it would nonetheless be valuable to conduct a sensitivity analysis regarding domain selection. Although this analysis is beyond the scope of this paper, we plan to address it in future studies.

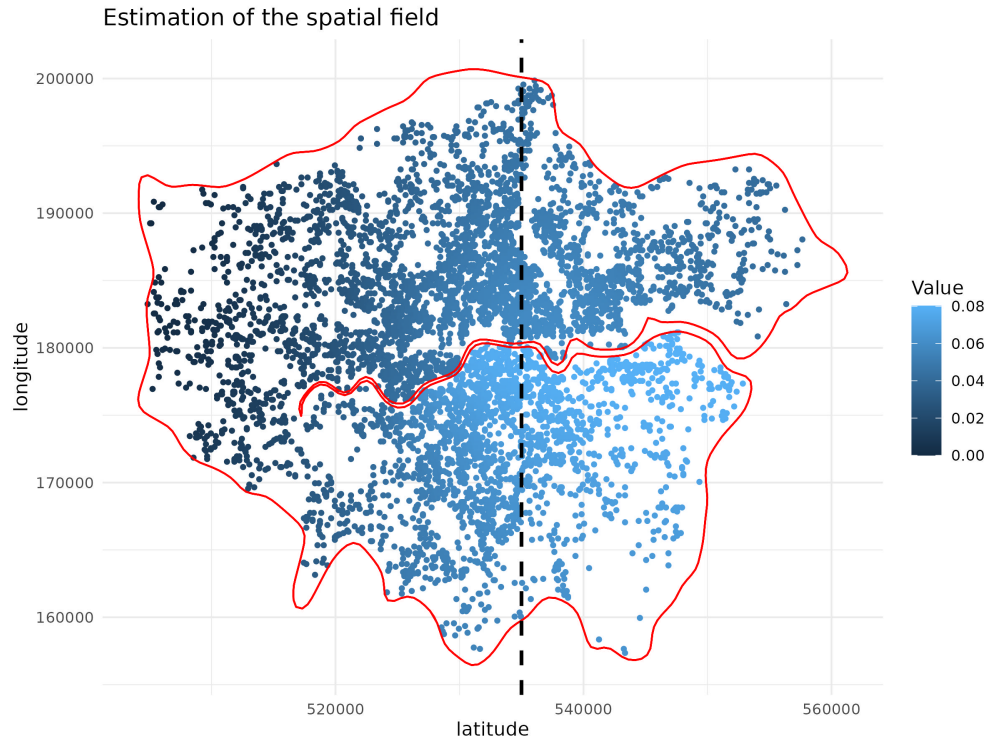


Figure 6: Estimated spatial field of fire engine response. The red contour outlines areas where geographical boundaries, particularly the River Thames, influence the response efficiency of fire engines. The vertical dotted line corresponds to the section considered in Figure 7

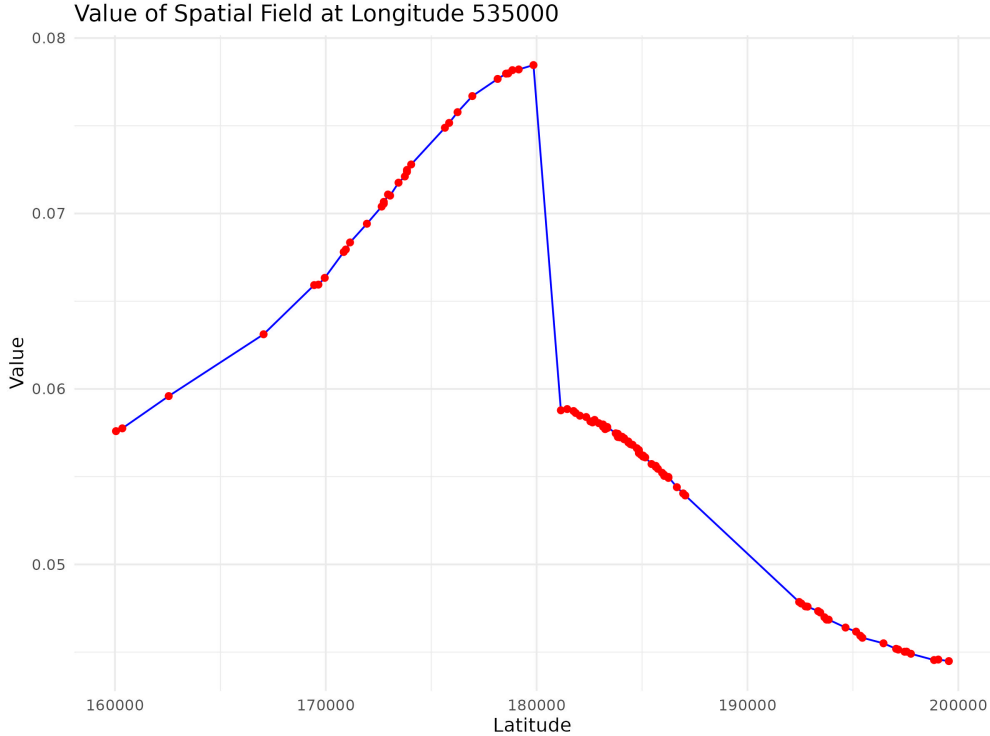


Figure 7: Estimated spatial field at Latitude 535000, where it is possible to observe a change point at Latitude 180000 corresponding to the presence of the river.

8 Conclusions

This paper introduces a novel SPH model that integrates differential regularization and the finite element method to effectively address spatial dependencies in survival data observed over irregular domains. Our methodology expands on the traditional semiparametric proportional hazards model by incorporating a non-parametric spatial field component to account for spatial dependence, providing a flexible approach to capture unobserved geographical heterogeneity in hazard rates across a spatial domain.

The SPH model framework offers several advantages over existing methods. First, our approach employs differential regularization, which controls the smoothness of the estimated spatial field, allowing for adaptation to complex spatial boundaries. Secondly, by applying the finite element method on triangulated spatial meshes, we achieve computationally efficient and accurate estimates, particularly in irregularly shaped regions where spatial dependencies do not follow straightforward geometric patterns.

The proposed model demonstrated promising results in both simulation and empirical studies. Simulations confirmed that the model yields accurate estimates of both the covariate effects and the spatial component across various sample sizes and levels of censoring.

In future work, we aim to enhance the model's adaptability by investigating alternative penalty structures, including anisotropic differential penalties, to more accurately capture directional dependencies in specific spatial datasets. Additionally, further research will focus on the asymptotic properties of the estimators to strengthen the model's theoretical foundations. Sensitivity analysis concerning the choice of the boundary domain will also be pursued. Finally, we plan to extend the model to incorporate time-varying covariates within the spatial proportional hazards framework, enabling application to more dynamic spatial survival contexts, such as real-time risk prediction and event-driven spatial analysis.

A Functional PIRLS Algorithm details

The maximizer $(\hat{\boldsymbol{\beta}}, \hat{f})$ of (4) must satisfy the following system of first-order equations:

$$\begin{cases} \frac{\partial \mathcal{L}(\hat{\boldsymbol{\beta}}, \hat{f})}{\partial \beta_k} = 0, & \forall k = 1, \dots, q, \\ \lim_{\tau \rightarrow 0} \frac{1}{\tau} \left[\mathcal{L}(\hat{\boldsymbol{\beta}}, \hat{f} + \tau u) - \mathcal{L}(\hat{\boldsymbol{\beta}}, \hat{f}) \right] - \mu m(u, \hat{f}) = 0, & \forall u \in \mathcal{F}. \end{cases} \quad (12)$$

This system involves derivatives with respect to both parameters $\boldsymbol{\beta}$ and f , where the derivative with respect to f is the Gâteaux derivative in the direction of $u \in \mathcal{F}$.

For each $k = 1, \dots, q$, the term $\frac{\partial \mathcal{L}(\hat{\boldsymbol{\beta}}, \hat{f})}{\partial \beta_k}$ is given by:

$$\frac{\partial \mathcal{L}(\hat{\boldsymbol{\beta}}, \hat{f})}{\partial \beta_k} = \sum_{i:\delta_i=1} \left(x_{ik} - \frac{\sum_{j:y_j \geq y_i} \exp(\mathbf{x}_j^\top \hat{\boldsymbol{\beta}} + \hat{f}(p_j)) \mathbf{x}_{jk}}{\sum_{j:y_j \geq y_i} \exp(\mathbf{x}_j^\top \hat{\boldsymbol{\beta}} + \hat{f}(p_j))} \right). \quad (13)$$

For the second equation of (12), we note that $m(u, \hat{f})$ is the derivative of $m(\hat{f}, \hat{f})$. We now compute the terms involving \mathcal{L} only:

$$\begin{aligned} \mathcal{L}(\hat{\boldsymbol{\beta}}, \hat{f} + \tau u) - \mathcal{L}(\hat{\boldsymbol{\beta}}, \hat{f}) &= \sum_{i:\delta_i=1} \left(tu(p_i) - \log \frac{\sum_{j:y_j \geq y_i} \exp(\mathbf{x}_j^\top \hat{\boldsymbol{\beta}} + \hat{f}(p_i) + tu(p_i))}{\sum_{j:y_j \geq y_i} \exp(\mathbf{x}_j^\top \hat{\boldsymbol{\beta}} + \hat{f}(p_j))} \right) \\ &= \sum_{i:\delta_i=1} \left(tu(p_i) - \log \frac{\sum_{j:y_j \geq y_i} \exp(\mathbf{x}_j^\top \hat{\boldsymbol{\beta}} + \hat{f}(p_j)) (1 + tu(p_i) + o(t))}{\sum_{j:y_j \geq y_i} \exp(\mathbf{x}_j^\top \hat{\boldsymbol{\beta}} + \hat{f}(p_j))} \right) \\ &= \sum_{i:\delta_i=1} \left(tu(p_i) - \log \left\{ 1 + t \frac{\sum_{j:y_j \geq y_i} \exp(\mathbf{x}_j^\top \hat{\boldsymbol{\beta}} + \hat{f}(p_j)) u(p_i)}{\sum_{j:y_j \geq y_i} \exp(\mathbf{x}_j^\top \hat{\boldsymbol{\beta}} + \hat{f}(p_j))} + o(t) \right\} \right) \\ &= \sum_{i:\delta_i=1} \left(tu(p_i) - t \frac{\sum_{j:y_j \geq y_i} \exp(\mathbf{x}_j^\top \hat{\boldsymbol{\beta}} + \hat{f}(p_j)) u(p_i)}{\sum_{j:y_j \geq y_i} \exp(\mathbf{x}_j^\top \hat{\boldsymbol{\beta}} + \hat{f}(p_j))} + o(t) \right). \end{aligned}$$

Thus, we obtain:

$$\lim_{\tau \rightarrow 0} \frac{1}{\tau} \left[\mathcal{L}(\hat{\boldsymbol{\beta}}, \hat{f} + \tau u) - \mathcal{L}(\hat{\boldsymbol{\beta}}, \hat{f}) \right] = \sum_{i:\delta_i=1} \left(u(p_i) - \frac{\sum_{j:y_j \geq y_i} \exp(\mathbf{x}_j^\top \hat{\boldsymbol{\beta}} + \hat{f}(p_j)) u(p_i)}{\sum_{j:y_j \geq y_i} \exp(\mathbf{x}_j^\top \hat{\boldsymbol{\beta}} + \hat{f}(p_j))} \right). \quad (14)$$

Define the following quantities:

$$\begin{aligned} \theta_i(\boldsymbol{\beta}, f) &= \exp(\mathbf{x}_i^\top \boldsymbol{\beta} + f(p_i)), \\ r_{ji} &= I(Y_j \geq Y_i), \\ s_i(\boldsymbol{\beta}, f) &= \sum_{j=1}^n r_{ji} \theta_j(\boldsymbol{\beta}, f). \end{aligned}$$

Thus, (13) can be rewritten as:

$$\begin{aligned}
\frac{\partial \mathcal{L}(\boldsymbol{\beta}, f)}{\partial \beta_k} &= \sum_{i=1}^n \delta_i x_{ik} - \sum_{i=1}^n \frac{\delta_i}{s_i(\boldsymbol{\beta}, f)} \sum_{j=1}^n r_{ji} \theta_j(\boldsymbol{\beta}, f) \mathbf{x}_{jk} \\
&= \sum_{i=1}^n \delta_i x_{ik} - \sum_{j=1}^n \theta_j(\boldsymbol{\beta}, f) \mathbf{x}_{jk} \sum_{i=1}^n r_{ji} \frac{\delta_i}{s_i(\boldsymbol{\beta}, f)} \\
&= \sum_{i=1}^n \delta_i x_{ik} - \sum_{i=1}^n \theta_i(\boldsymbol{\beta}, f) x_{ik} l_i(\boldsymbol{\beta}, f) \\
&= \sum_{i=1}^n (\delta_i - \theta_i(\boldsymbol{\beta}, f) l_i(\boldsymbol{\beta}, f)) \mathbf{x}_{ik},
\end{aligned}$$

where $l_i(\boldsymbol{\beta}, f) = \sum_{j=1}^n r_{ij} \frac{\delta_j}{s_j(\boldsymbol{\beta}, f)}$. Continuing, we have:

$$\begin{aligned}
\frac{\partial \mathcal{L}(\boldsymbol{\beta}, f)}{\partial \beta_k} &= \sum_{i=1}^n \frac{l_i(\boldsymbol{\beta}, f)^{-1} \delta_i - \theta_i(\boldsymbol{\beta}, f)}{\theta_i(\boldsymbol{\beta}, f) l_i(\boldsymbol{\beta}, f)^{-1}} \theta_i(\boldsymbol{\beta}, f) x_{ik} \\
&= \sum_{i=1}^n \frac{l_i(\boldsymbol{\beta}, f)^{-1} \delta_i - \theta_i(\boldsymbol{\beta}, f)}{\theta_i(\boldsymbol{\beta}, f) l_i(\boldsymbol{\beta}, f)^{-1}} \frac{\partial \theta_i(\boldsymbol{\beta}, f)}{\partial \beta_k}.
\end{aligned}$$

Similarly, the Gâteaux derivative of $\mathcal{L}(\boldsymbol{\beta}, f)$ in the direction u is:

$$\frac{\partial \mathcal{L}(\boldsymbol{\beta}, u)}{\partial f} = \sum_{i=1}^n \frac{l_i^{-1} \delta_i - \theta_i(\boldsymbol{\beta}, f)}{v_i} \frac{\partial \theta_i(\boldsymbol{\beta}, u)}{\partial f}.$$

Thus, solving (12) is equivalent to finding $(\hat{\boldsymbol{\beta}}, \hat{f})$ that satisfies:

$$\begin{cases} \sum_{i=1}^n \frac{l_i^{-1} \delta_i - \theta_i(\boldsymbol{\beta}, f)}{v_i} \frac{\partial \theta_i(\boldsymbol{\beta}, f)}{\partial \beta_k} = 0, & \forall k = 1, \dots, q, \\ \sum_{i=1}^n \frac{l_i^{-1} \delta_i - \theta_i(\boldsymbol{\beta}, f)}{v_i} \frac{\partial \theta_i(\boldsymbol{\beta}, u)}{\partial f} + \mu m(u, \hat{f}) = 0, & \forall u \in \mathcal{F}. \end{cases} \quad (15)$$

Assuming l_i and v_i are constant, solving (15) is equivalent to finding the minimizer of the functional:

$$\mathcal{J}_\mu(\boldsymbol{\beta}, f) = \|V^{-1/2}(\boldsymbol{\delta}/\mathbf{l} - \boldsymbol{\theta})\|^2 + \mu m(f, f),$$

where $\boldsymbol{\delta}/\mathbf{l} = (\delta_1/l_1, \dots, \delta_n/l_n)^\top$, $\mathbf{v} = (v_1, \dots, v_n)^\top$, $V = \text{diag}(\mathbf{v})$ and diag denotes a diagonal matrix with the \mathbf{v} elements along its main diagonal, and zeros elsewhere. Assuming such quantities are constant suggests an iterative computation scheme.

Let $\boldsymbol{\theta}^{(k)}$ be an estimate of $\boldsymbol{\theta}(\boldsymbol{\beta}, f)$ after k iterations. We consider a first-order approximation of $\boldsymbol{\theta}$ near the current value $\boldsymbol{\theta}^{(k)} = (\boldsymbol{\beta}^{(k)}, f^{(k)})$:

$$\boldsymbol{\theta}(\boldsymbol{\beta}, f) \approx \underbrace{\exp(X\boldsymbol{\beta}^{(k)} + f^{(k)})}_{\boldsymbol{\theta}^{(k)}} + \frac{\partial \boldsymbol{\theta}(\boldsymbol{\beta}, f)}{\partial \boldsymbol{\beta}} (\boldsymbol{\beta} - \boldsymbol{\beta}^{(k)}) + \frac{\partial \boldsymbol{\theta}(\boldsymbol{\beta}, f)}{\partial f} (f - f^{(k)}).$$

The partial derivatives of $\boldsymbol{\theta}$ with respect to both parameters are computed as follows. For the derivative with respect to $\boldsymbol{\beta}$:

$$\frac{\partial \theta_i^{(k)}}{\partial \beta_j} = \theta_i^{(k)} x_{ij},$$

which in matrix form is:

$$\frac{\partial \boldsymbol{\theta}(\boldsymbol{\beta}, f)}{\partial \boldsymbol{\beta}} = \boldsymbol{\Theta}^{(k)} X,$$

where $\boldsymbol{\Theta}^{(k)} = \text{diag}(\boldsymbol{\theta}^{(k)})$.

Similarly, for the derivative with respect to f , we have:

$$\frac{\partial \theta_i(\boldsymbol{\beta}^{(k)}, f^{(k)} + \tau(f - f^{(k)}))}{\partial f} = \theta_i(\boldsymbol{\beta}^{(k)}, f^{(k)})(f(p_i) - f^{(k)}(p_i)).$$

Hence, the first-order approximation of $\mathcal{J}_\mu(\boldsymbol{\beta}, f)$ in the neighborhood of $(\boldsymbol{\beta}^{(k)}, f^{(k)})$ is:

$$\begin{aligned} \tilde{\mathcal{J}}_\lambda^{(k)}(\boldsymbol{\beta}, f) &= \left\| V^{-1/2} \left[\boldsymbol{\delta}/l - \left(\boldsymbol{\theta}^{(k)} + \Theta^{(k)} X(\boldsymbol{\beta} - \boldsymbol{\beta}^{(k)}) + \Theta^{(k)}(f - f^{(k)}) \right) \right] \right\|^2 + \mu m(f, f) \\ &= \left\| V^{-1/2} \Theta^{(k)} \left((\Theta^{(k)})^{-1}(\boldsymbol{\delta}/l - \boldsymbol{\theta}^{(k)}) + X\boldsymbol{\beta}^{(k)} + f^{(k)} - X\boldsymbol{\beta} - f \right) \right\|^2 + \mu m(f, f). \end{aligned}$$

Defining $\mathbf{z}^{(k)} = (\Theta^{(k)})^{-1}(\boldsymbol{\delta}/l - \boldsymbol{\theta}^{(k)}) + X\boldsymbol{\beta}^{(k)} + f^{(k)}$, and letting $W^{(k)}$ be the $n \times n$ diagonal matrix with i th entry equal to $v_i^{-1}(\boldsymbol{\beta}^{(k)}, f^{(k)})\theta_i^2(\boldsymbol{\beta}^{(k)}, f^{(k)})$, we can rewrite:

$$\tilde{\mathcal{J}}_\lambda^{(k)}(\boldsymbol{\beta}, f) = \left\| (W^{(k)})^{1/2}(\mathbf{z}^{(k)} - X\boldsymbol{\beta} - f) \right\|^2 + \mu m(f, f). \quad (16)$$

Since $W^{(k)}$ is positive definite, $\tilde{\mathcal{J}}_\lambda$ is a quadratic form with a unique minimum.

B Proof of Proposition 1

The proof of Proposition 1 follows the approach outlined in Appendix C of Sangalli et al. (2013). We begin by recalling the Lax-Milgram theorem (Quarteroni and Quarteroni, 2009).

Theorem 1 (Lax-Milgram). *Let \mathcal{F} be a Hilbert space, $G(\cdot, \cdot) : \mathcal{F} \times \mathcal{F} \rightarrow \mathbb{R}$ a continuous and coercive bilinear form, and $F : \mathcal{F} \rightarrow \mathbb{R}$ a linear and continuous functional. Then, there exists a unique solution to the following problem:*

$$\text{find } u \in \mathcal{F} \text{ such that } G(u, v) = F(v), \quad \forall v \in \mathcal{F}.$$

Moreover, if $G(\cdot, \cdot)$ is symmetric, then $u \in \mathcal{F}$ is the unique minimizer in \mathcal{F} of the functional $B : \mathcal{F} \rightarrow \mathbb{R}$, defined as

$$B(u) = G(u, u) - 2F(u).$$

We also require the following result.

Lemma 1. *The bilinear and symmetric form $G : H_{n0}^2(\Omega) \times H_{n0}^2(\Omega) \rightarrow \mathbb{R}$, defined as*

$$G(v, u) = \mathbf{u}_n^\top Q \mathbf{v}_n + \lambda \int_{\Omega} (\Delta u)(\Delta v),$$

is continuous and coercive.

Proof. We recall the definitions of the norm $\|\cdot\|_{H^2}$ and the semi-norm $|\cdot|_{H^2}$:

$$\|u\|_{H^2} = \sum_{|\alpha| \leq 2} \|\partial^\alpha u\|_{L^2}, \quad |u|_{H^2} = \|\Delta u\|_{L^2}, \quad \forall u \in H^2.$$

First, note that the semi-norm $|\cdot|_{H^2}$ and the norm $\|\cdot\|_{H^2}$ are equivalent in $H_{n0}^2(\Omega)$ (Quarteroni and Quarteroni, 2009), i.e., there exists $C_0 > 0$ such that $|u|_{H^2(\Omega)} \geq C_0 \|u\|_{H^2(\Omega)}$, $\forall u \in H_{n0}^2(\Omega)$. Then, we have:

$$G(u, u) = \mathbf{u}_n^\top Q \mathbf{u}_n + \lambda \int_{\Omega} (\Delta u)^2 \geq \lambda \int_{\Omega} (\Delta u)^2 = \lambda |u|_{H^2(\Omega)}^2 \geq \lambda C_0 \|u\|_{H^2(\Omega)}^2;$$

thus, $G(\cdot, \cdot)$ is coercive.

We now show the continuity of $G(\cdot, \cdot)$. Since $H^2(\Omega) \subset C^0(\Omega)$ and since the norms $\|\cdot\|_\infty$ and $\|\cdot\|_2$ are equivalent on \mathbb{R}^n , there exists a constant C_1 such that $\|\mathbf{v}_n\|_\infty \leq C_1 \|v\|_{H^2(\Omega)}$, $\forall v \in H^2(\Omega)$. Since Q is symmetric, its largest eigenvalue ρ is non-negative. Then we have:

$$G(u, v) = \mathbf{u}_n^\top Q \mathbf{v}_n + \lambda \int_{\Omega} (\Delta u)(\Delta v) \leq \rho \|\mathbf{u}_n\|_\infty \|\mathbf{v}_n\|_\infty + \lambda |u|_{H^2(\Omega)} |v|_{H^2(\Omega)} \leq \max\{\rho C_1^2, \lambda C_0^2\} \|u\|_{H^2(\Omega)} \|v\|_{H^2(\Omega)}.$$

Hence, the bilinear form $G(\cdot, \cdot)$ is also continuous. \square

We can now provide the proof of Proposition 1.

Proof. First, given $f \in H_{n0}^2$, the unique minimizer of the functional $\tilde{J}_\lambda(\beta, f)$ is given by:

$$\tilde{\beta}(f) = (X^\top W X)^{-1} X^\top W (z - \mathbf{f}_n).$$

To show this, we take the derivative of $\tilde{J}_\lambda(\beta, f)$ with respect to β :

$$\frac{\partial \tilde{J}_\lambda(\beta, f)}{\partial \beta} = -2X^\top W (z - \mathbf{f}_n) + (X^\top W X)\beta.$$

Since X is a full-rank matrix and W is invertible (each diagonal entry of W is strictly positive by construction), $X^\top W X$ is also invertible. Finally, the necessary condition $\frac{\partial \tilde{J}_\lambda(\tilde{\beta}, f)}{\partial \beta} = 0$ is satisfied if and only if $\tilde{\beta}$ is given by the above expression. Since for fixed f , $\tilde{J}_\lambda(\beta, f)$ is clearly convex, $\tilde{\beta}$ is indeed a minimum.

Substituting $\tilde{\beta}$ into the objective function, we obtain the following form of the functional:

$$\tilde{J}_\lambda(f) = z^\top Q z - 2\mathbf{f}_n^\top Q z + \mathbf{f}_n^\top Q \mathbf{f}_n + \lambda \int_{\Omega} (\Delta f)^2.$$

To optimize this functional with respect to f alone, the problem reduces to finding $\tilde{f} \in H_{n0}^2$ that minimizes:

$$J_\lambda^*(f) = \mathbf{f}_n^\top Q \mathbf{f}_n + \lambda \int_{\Omega} (\Delta f)^2 - 2\mathbf{f}_n^\top Q z.$$

We can express $J_\lambda^*(f) = G(f, f) - 2F(f)$, where

$$G(u, v) = \mathbf{u}_n^\top Q \mathbf{v}_n + \lambda \int_{\Omega} (\Delta u)(\Delta v) \quad \text{and} \quad F(v) = \mathbf{v}_n^\top Q z.$$

Lemma 1 ensures that $G(\cdot, \cdot)$ is a coercive and continuous bilinear form on $H_{n0}^2 \times H_{n0}^2$; moreover, F is trivially a linear and continuous functional on H_{n0}^2 . By applying the Lax-Milgram Theorem and leveraging the symmetry of $G(\cdot, \cdot)$, the minimizer of the functional J_λ^* is the function $\tilde{f} \in H_{n0}^2$ such that

$$\mathbf{u}_n^\top Q \tilde{\mathbf{f}}_n + \lambda \int_{\Omega} (\Delta u)(\Delta \tilde{f}) = \mathbf{u}_n^\top Q z, \quad \forall u \in H_{n0}^2.$$

Thus, we conclude that \tilde{f} exists and is unique, and consequently, $\tilde{\beta}$ also exists and is unique. \square

References

- Azzimonti, L., Nobile, F., Sangalli, L. M., and Secchi, P. (2014). Mixed finite elements for spatial regression with pde penalization. *SIAM/ASA Journal on Uncertainty Quantification*, 2(1):305–335.
- Cox, D. R. (1972). Regression models and life-tables. *Journal of the Royal Statistical Society: Series B (Methodological)*, 34(2):187–202.
- Cygu, S., Dushoff, J., and Bolker, B. M. (2021). pcoxtime: Penalized cox proportional hazard model for time-dependent covariates. *arXiv preprint arXiv:2102.02297*.
- Dai, B. and Breheny, P. (2019). Cross validation approaches for penalized cox regression. *arXiv preprint arXiv:1905.10432*.
- Deresa, N. W. and Keilegom, I. V. (2024). Copula based cox proportional hazards models for dependent censoring. *Journal of the American Statistical Association*, 119(546):1044–1054.
- Fire, L. and Authority, E. P. (2015). London Fire Brigade Incident Records. London Datastore. <http://data.london.gov.uk/dataset/london-fire-brigade-incident-records>.

- Hanson, T. and Zhou, H. (2014). Spatial survival model. *Wiley StatsRef: Statistics Reference Online*, pages 1–8.
- Harrell Jr, F. E., Lee, K. L., and Mark, D. B. (1996). Multivariable prognostic models: issues in developing models, evaluating assumptions and adequacy, and measuring and reducing errors. *Statistics in medicine*, 15(4):361–387.
- Li, Y. and Lin, X. (2006). Semiparametric normal transformation models for spatially correlated survival data. *Journal of the American Statistical Association*, 101(474):591–603.
- O’sullivan, F., Yandell, B. S., and Raynor Jr, W. J. (1986). Automatic smoothing of regression functions in generalized linear models. *Journal of the American Statistical Association*, 81(393):96–103.
- Paik, J. and Ying, Z. (2012). A composite likelihood approach for spatially correlated survival data. *Computational statistics & data analysis*, 56(1):209–216.
- Quarteroni, A. and Quarteroni, S. (2009). *Numerical models for differential problems*, volume 2. Springer.
- Ramsay, T. (2002). Spline smoothing over difficult regions. *Journal of the Royal Statistical Society Series B: Statistical Methodology*, 64(2):307–319.
- Sangalli, L. M., Ramsay, J. O., and Ramsay, T. O. (2013). Spatial spline regression models. *Journal of the Royal Statistical Society Series B: Statistical Methodology*, 75(4):681–703.
- Shewchuk, J. R. (2002). Delaunay refinement algorithms for triangular mesh generation. *Computational geometry*, 22(1-3):21–74.
- Taylor, B. M. (2017). Spatial modelling of emergency service response times. *Journal of the Royal Statistical Society Series A: Statistics in Society*, 180(2):433–453.
- Taylor, B. M. and Rowlingson, B. S. (2017). spatsurv: an r package for bayesian inference with spatial survival models. *Journal of Statistical Software*, 77:1–32.
- Therneau, T. et al. (2015). A package for survival analysis in s. *R package version*, 2(7):2014.
- Wilhelm, M. and Sangalli, L. M. (2016). Generalized spatial regression with differential regularization. *Journal of Statistical Computation and Simulation*, 86(13):2497–2518.
- Wood, S. N., Bravington, M. V., and Hedley, S. L. (2008). Soap film smoothing. *Journal of the Royal Statistical Society Series B: Statistical Methodology*, 70(5):931–955.